 CMES, vol.30, no.2, pp.77-97, 2008

Thermal Analysis of Reissner-Mindlin Shallow Shells with FGM Properties by the MLPG

J. Sladek[1], V. Sladek[1], P. Solek[2], P.H. Wen[3] and S.N. Atluri[4]

Abstract: A meshless local Petrov-Galerkin (MLPG) method is applied to solve problems of Reissner-Mindlin shells under thermal loading. Both stationary and thermal shock loads are analyzed here. Functionally graded materials with a continuous variation of properties in the shell thickness direction are considered here. A weak formulation for the set of governing equations in the Reissner-Mindlin theory is transformed into local integral equations on local subdomains in the base plane of the shell by using a unit test function. Nodal points are randomly spread on the surface of the plate and each node is surrounded by a circular subdomain to which local integral equations are applied. The meshless approximation based on the Moving Least-Squares (MLS) method is employed for the implementation.

Keyword: Meshless local Petrov-Galerkin method (MLPG), Moving least-squares (MLS) approximation, functionally graded materials, thermal load

1 Introduction

In recent years, the demand for construction of huge and lightweight shell and spatial structures is increasing. To minimize the weight of shell structures a layered profile of the shell is utilized frequently. In such a case a delamination of individual layers may occur due to a finite jump in the material properties across the layer-interfaces. To alleviate this phenomenon, functionally graded materials (FGMs) are often introduced [Suresh and Mortensen, 1998; Miyamoto et al., 1999]. FGMs are multi-phase materials with a pre-determined property profile, whereby the phase volume fractions are varying gradually in space. This results in continuously non-homogenous material properties at the macroscopic structural scale. Often, these spatial gradients in the material behaviour render FGMs to be superior to conventional composites because of their continuously graded structures and properties. FGMs may exhibit isotropic or anisotropic material properties, depending on the processing technique and the practical engineering requirements.

Many linear analyses of bending of shells are focused only on a lateral pressure loading, with the assumption of uniformly distributed temperature in the whole shell. However, shells with FGM properties are frequently under a thermal load. Therefore, it is interesting to analyze shells under a general thermal load. Literature sources on this subject are very limited, and they are mostly restricted to analyses of plates. An elegant introduction and overview of pioneering efforts in thermal stress analyses was given by Boley and Weiner (1960). Later Tauchert (1991) gave a comprehensive overview of thermally induced flexure, buckling and vibration of plates described by the Kirchhoff theory. Thermoelastic analyses including transverse shear effects were performed by Das and Rath (1972) and Bapu Rao (1979). Nonlinear analysis of simply supported Reissner-Mindlin plates subjected to lateral pressure and thermal loading and resting on two-parameter elastic foundations is given by Shen (2000). Praveen and Reddy (1998) analyzed the

[1] Institute of Construction and Architecture, Slovak Academy of Sciences, 84503 Bratislava, Slovakia
[2] Department of Mechanics, Slovak Technical University, Bratislava, Slovakia
[3] School of Engineering and Materials Sciences, Queen Mary University of London, Mile End, London E14NS, U.K.
[4] Department of Mechanical and Aerospace Engineering, University of California at Irvine, Irvine, CA 92697, USA.

thermomechanical response of thick plates with continuous variation of properties through the plate thickness. The FEM has been applied to isotropic plates with a simple power law distribution of ceramic and metallic constituents. Vel and Batra (2002) obtained an exact solution for three-dimensional deformations of a simply supported functionally graded rectangular plates subjected to mechanical and thermal loads on its top and bottom surfaces.

Due to the high mathematical complexity of the boundary or initial-boundary value problems, analytical approaches for FGMs are restricted to simple geometries and boundary conditions. The choice of an appropriate mathematical model together with a consistent computational method is important for such kind of structures. Most significant advances in shell analyses have been made using the finite element method (FEM). It is well known that standard displacement-based type shell element is too stiff and thus suffers from locking phenomena. Locking problem arises due to inconsistencies in discrete representation of the transverse shear energy and membrane energy [Dvorkin and Bathe, 1984]. Much effort has been devoted to deriving shell elements which account for the out-of-plane shear deformation in thick shells that are free from locking in the thin shell limit. In view of the increasing reliability on the use of computer modelling to replace or reduce experimental works in the context of a virtual testing, it is therefore imperative that alternative computer-based methods are developed to allow for independent verification of the finite element solutions [Arciniega and Reddy, 2007].

The boundary element method (BEM) has emerged as an alternative numerical method to solve plate and shell problems. A review on early applications of BEM to shells is given by Beskos (1991). The first application of BEM to shells is given by Newton and Tottenham (1968), where they presented a method based on the decomposition of the fourth-order governing equation into a set of the second-order ones. Lu and Huang (1992) derived a direct BEM formulation for shallow shells involving shear deformation. For elastodynamic shell problems it is appropriate to use the weighted residual method with the static fundamental solution as a test function [Zhang and Atluri (1986), Providakis and Beskos (1991)]. Dirgantara and Aliabadi (1999) applied the domain-boundary element method for shear deformable shells under a static load. They used a test function corresponding to the thick plate bending problem. Ling and Long (1996) used this method for geometrically non-linear analysis of shallow shells. All previous BEM applications are dealing with isotropic shallow shells. Only Wang and Schweizerhof (1996a,b) applied a boundary integral equation method for moderately thick laminated orthotropic shallow shells. They used the static fundamental solution corresponding to a shear deformable orthotropic shell and applied it for free vibration analysis of thick shallow shells. The fundamental solution for a thick orthotropic shell under a dynamic load is not available according to the best of the author's knowledge.

Meshless approaches for problems of continuum mechanics have attracted much attention during the past decade [Belytschko et al., (1996), Atluri (2004)]. In spite of the great success of the FEM and the BEM as accurate and effective numerical tools for the solution of boundary value problems with complex domains, there is still a growing interest in developing new advanced numerical methods. Elimination of shear locking in thin walled structures by standard FEM is difficult and techniques developed are not accurate. However, the FEM based on the mixed approximations with the reduced integration performs quite well. Meshless methods with continuous approximation of stresses are more convenient for such kinds of structures [Donning and Liu (1998)]. In recent years, meshfree or meshless formulations are becoming to be popular due to their high adaptivity and low costs to prepare input data for numerical analyses. Many of meshless methods are derived from a weak-form formulation on global domain or a set of local subdomains. In the global formulation background cells are required for the integration of the weak-form. It should be noticed that integration is performed only on those background cells with a nonzero shape function.

In methods based on local weak-form formulation no cells are required. The first application of a meshless method to plate/shell problems was given by Krysl and Belytschko (1996a,b), where they applied the element-free Galerkin method. The moving least-square (MLS) approximation yields C^1 continuity which satisfies the Kirchhoff hypotheses. The continuity of the MLS approximation is given by the minimum between the continuity of the basis functions and that of the weight function. So continuity can be tuned to a desired value. Their results showed excellent convergence, however, their formulation is not applicable to shear deformable plate/shell problems. Recently, Noguchi et al. (2000) used a mapping technique to transform the curved surface into flat two-dimensional space. Then, the element-free Galerkin method can be applied also to thick plates or shells including the shear deformation effects. The reproducing kernel particle method (RKPM) [Liu et al. (1995)] has been successfully applied for large deformations of thin isotropic shells [Li et al. (2000)].

One of the most rapidly developed meshfree methods is the Meshless Local Petrov-Galerkin method (MLPG)[Atluri and Zhu(1998)]. The MLPG method has attracted much attention during the past decade [Atluri and Shen, 2002; Atluri, 2004; Atluri et al., 2003; Sellountos et al., 2005] for many problems of continuum mechanics. Recent successes of the MLPG methods have been reported in solving a 4^{th} order ordinary differential equation [Atluri and Shen (2005)]; in analyzing vibrations of a beam with multiple cracks [Andreaus et al (2005)]; in the development of the MLPG finite-volume mixed method{ Atluri, Han , and Rajendran (2004)], which was later extended to finite deformation analysis of static and dynamic problems [Han et al (2005)]; in simplified treatment of essential boundary conditions by a novel modified MLS procedure [Gao et al (2006)]; in application to solving the Q-tensor equations of nematostatics [Pecher et al (2006)]; in analysis of transient thermomechanical response of functionally gradient composites [Ching and Chen (2006)]; in the ability for solving high-speed contact, impact and penetration problems with large deformations and rotations [Han et al (2006)]; in the development of the mixed scheme to interpolate the elastic displacements and stresses independently [Atluri et al (2006a), (2006b)]; in proposal of a direct solution method for the quasi-unsymmetric sparse matrix arising in the MLPG [Yuan et al (2007)]; in modelling nonlinear water waves [Ma (2007)]; in the development of the MLPG with using the Dirac delta function as the test function for 2D heat conduction problems in irregular domain [Wu et al (2007)]; for studying the diffusion of a magnetic field within a non-magnetic conducting medium with nonhomogeneous and anisotropic electrical resistivity [Johnson and Owen (2007)]; in the development of the MLPG with using simplified finite difference interpolation [Ma (2008)] and in 3-D modelling of homogeneous shells under a mechanical load [Jarak et al. (2007)]. The MLPG Mixed Finite Volume Method [Atluri, Han, and Rajendran (2004) has proved to be an effective way in eliminating shear and thickness locking in shells [Jarak et al (2007)], and in eliminating locking and the necessity for upwinding in solving convection dominated flows of incompressible fluids [Han and Atluri (2008a,b)].

In the present paper, the authors have developed a meshless method based on the local Petrov-Galerkin weak-form to solve thermal problems of orthotropic thick shells with material properties continuously varying through the shell thickness. The Reissner-Mindlin theory [Reissner (1945), Mindlin (1951)] reduces the original 3-d thick plate problem to a 2-d problem. Nodal points are randomly distributed over the base plane of the considered shell. Each node is the center of a circle surrounding this node. Similar approach has been successfully applied to a thin Kirchhoff plate [Long and Atluri, 2002; Sladek et al., 2002, 2003]. The MLPG method has been also applied to Reissner-Mindlin plates under dynamic load by Sladek et al. (2007a). Soric et al. (2004) have performed a three-dimensional analysis of thick plates, where a plate is divided by small cylindrical subdomains for which the MLPG is applied. Homogeneous material properties of plates are considered in previous papers. Recently, Qian

et al. (2004) extended the MLPG for 3-D deformations in thermoelastic bending of functionally graded isotropic plates. The MLPG has been successfully applied also to shell with homogeneous [Sladek et al. (2007b)] and FGM properties [Sladek et al. (2008a)] under a mechanical load.

The solution of the uncoupled problem in the present paper is split into two tasks. In the first task the temperature distribution in the shell has to be obtained by solving the diffusion equation. The temperature distribution in shell has to be analyzed as 3-D problem. The MLPG is applied to transient heat conduction equations in a continuously nonhomogeneous solid. The Laplace transform technique is used to eliminate the time variable too. Several quasi-static boundary value problems must be solved for various values of the Laplace-transform parameter. The Stehfest's inversion method [Stehfest, 1970] is applied to obtain the time-dependent solution. In the second task the set of governing differential equations for Reissner-Mindlin shell bending theory with Duhamel-Neumann constitutive equations is solved. Since thermal changes in solids are relatively slow with respect to the elastic wave velocity, the inertial terms in Reissner-Mindlin governing equations are not considered. The problem is considered as a quasi-static with time dependent thermal forces. The MLPG method is applied again to the solution of that problem with the meshless Moving Least-Squares (MLS) approximation of primary field variables. The nodal points are spread freely in the analyzed domain and on its boundary. The essential boundary conditions are satisfied by collocation of approximated fields at nodes with prescribed values. In other nodes, the governing PDEs are considered on subdomains around these nodes in the local weak-form with the use of unit test functions. The resulting local integral equations are discretized within the assumed approximation of field variables. Numerical results for simply supported and clamped square shells with a uniform or sinusoidal temperature distribution on the top surface of the shell are presented to illustrate the accuracy and efficiency of the proposed method. A thermal shock with Heaviside time variation on the top surface of the simply supported shell is also analyzed. The comparisons of the present numerical results with FEM results show good agreement.

2 The MLS approximation

In general, a meshless method uses a local interpolation to represent the trial function with the values (or the fictitious values) of the unknown variable at some randomly spread nodes. The moving least squares approximation may be considered as one of such schemes, and is used in the current work. Consider a sub-domain Ω_x, the neighbourhood of a point x and denoted as the domain of definition of the MLS approximation for the trial function at $\mathbf{x}$, which is located in the problem domain Ω. To approximate the distribution of the function u in Ω_x, over a number of randomly located nodes $\{\mathbf{x}^a\}$, $a = 1,2,\ldots,n$, the MLS approximant $u^h(\mathbf{x})$ of u, $\forall \mathbf{x} \in \Omega_x$, can be defined by

$$u^h(\mathbf{x}) = \mathbf{p}^T(\mathbf{x})\mathbf{a}(\mathbf{x}) \quad \forall \mathbf{x} \in \Omega_x, \tag{1}$$

where $\mathbf{p}^T(\mathbf{x}) = \left[p^1(\mathbf{x}), p^2(\mathbf{x}), \ldots, p^m(\mathbf{x})\right]$ is a complete monomial basis of order m; and $\mathbf{a}(\mathbf{x})$ is a vector containing coefficients $a^j(\mathbf{x})$, $j = 1,2,\ldots,m$ which are functions of the space coordinates $\mathbf{x} = [x_1, x_2, x_3]^T$. For example, for a 2-d problem

$$\mathbf{p}^T(\mathbf{x}) = [1,\ x_1,\ x_2], \quad \text{linear basis } m = 3 \tag{2a}$$

$$\mathbf{p}^T(\mathbf{x}) = \left[1,\ x_1,\ x_2,\ (x_1)^2,\ x_1x_2,\ (x_2)^2\right], \quad \text{quadratic basis } m = 6 \tag{2b}$$

The coefficient vector $\mathbf{a}(\mathbf{x})$ is determined by minimizing a weighted discrete L_2 norm, defined as

$$J(\mathbf{x}) = \sum_{a=1}^{n} v^a(\mathbf{x}) \left[\mathbf{p}^T(\mathbf{x}^a)\mathbf{a}(\mathbf{x}) - \hat{u}^a\right]^2, \tag{3}$$

where $v^a(\mathbf{x})$ is the weight function associated with the node a, with $v^a(\mathbf{x}) \geq 0$. Recall that n is the number of nodes in $\Omega_x$for which the weight functions $v^a(\mathbf{x}) > 0$ and $\hat{u}^a$ are the fictitious nodal values, and not the nodal values of the unknown trial function $u^h(\mathbf{x})$ in general. The stationarity of J in

eq. (3) with respect to $\mathbf{a}(\mathbf{x})$ leads to the following linear relation between $\mathbf{a}(\mathbf{x})$ and $\hat{\mathbf{u}}$

$$\mathbf{A}(\mathbf{x})\mathbf{a}(\mathbf{x}) = \mathbf{B}(\mathbf{x})\hat{\mathbf{u}}, \tag{4}$$

where

$$\mathbf{A}(\mathbf{x}) = \sum_{a=1}^{n} w^a(\mathbf{x})\mathbf{p}(\mathbf{x}^a)\mathbf{p}^T(\mathbf{x}^a)$$

$$\mathbf{B}(\mathbf{x}) = \left[v^1(\mathbf{x})\mathbf{p}(\mathbf{x}^1), v^2(\mathbf{x})\mathbf{p}(\mathbf{x}^2), \ldots, v^n(\mathbf{x})\mathbf{p}(\mathbf{x}^n)\right]. \tag{5}$$

The MLS approximation is well defined only when the matrix $\mathbf{A}$ in eq. (4) is non-singular. A necessary condition to be satisfied that requirement is that at least m weight functions are non-zero (i.e. $n \geq m$) for each sample point $\mathbf{x} \in \Omega$ and that the nodes in Ω_x will not be arranged in a special pattern such as on a straight line.

Solving for $\mathbf{a}(\mathbf{x})$ from eq. (4) and substituting it into eq. (1) give a relation

$$\mathbf{u}^h(\mathbf{x}) = \Phi^T(\mathbf{x}) \cdot \hat{\mathbf{u}} = \sum_{a=1}^{n} \phi^a(\mathbf{x})\hat{u}^a; \quad \hat{u}^a \neq u(\mathbf{x}^a) \wedge \hat{u}^a \neq u^h(\mathbf{x}^a), \tag{6}$$

where

$$\Phi^T(\mathbf{x}) = \mathbf{p}^T(\mathbf{x})\mathbf{A}^{-1}(\mathbf{x})\mathbf{B}(\mathbf{x}). \tag{7}$$

$\phi^a(\mathbf{x})$ is usually called the shape function of the MLS approximation corresponding to the nodal point $\mathbf{x}^a$. From eqs (5) and (7), it may be seen that $\phi^a(\mathbf{x}) = 0$ when $v^a(\mathbf{x}) = 0$. In practical applications, $v^a(\mathbf{x})$ is generally chosen such that it is non-zero over the support domain of the nodal point $\mathbf{x}^a$. The support domain is usually taken to be circle of radius r^a centered at $\mathbf{x}^a$ (see Fig. 1). This radius is an important parameter of the MLS approximation because it determines the range of interaction (coupling) between degrees of freedom defined at nodes.

Both the Gaussian and spline weight functions with compact supports are most frequently used in numerical analyses. The Gaussian weight function can be written as

$$v^a(\mathbf{x}) = \begin{cases} \exp\left[-\left(\frac{d^a}{c^a}\right)^2\right] - \exp\left[-\left(\frac{r^a}{c^a}\right)^2\right], \\ \qquad\qquad 0 \leq d^a \leq r^a \\ 0, \qquad\qquad d^a \geq r^a \end{cases} \tag{8}$$

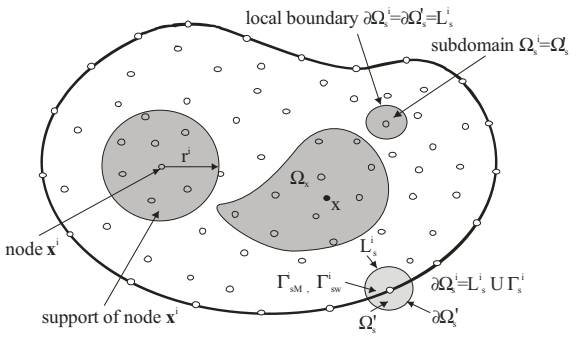

Figure 1: Local boundaries for weak formulation, the domain Ω_x for MLS approximation, and support area of weight function around node $\mathbf{x}^i$

where $d^a = |\mathbf{x} - \mathbf{x}^a|$; c^a is a parameter controlling the shape of the weight function v^a and r^a is the size of support. The radius of the support domain r^a should be large enough to have a sufficient number of nodes covered in the domain of definition to ensure the regularity of matrix $\mathbf{A}$.

A 4^{th}-order spline-type weight function

$$v^a(\mathbf{x}) = \begin{cases} 1 - 6\left(\frac{d^a}{r^a}\right)^2 + 8\left(\frac{d^a}{r^a}\right)^3 - 3\left(\frac{d^a}{r^a}\right)^4, \\ \qquad\qquad 0 \leq d^a \leq r^a, \\ 0, \qquad\qquad d^a \geq r^a, \end{cases} \tag{9}$$

is more convenient for modelling since the C^1-continuity of the weight function is ensured over the entire domain. Then, the continuity conditions for the bending moments, the shear forces and the normal forces are satisfied.

The partial derivatives of the MLS shape functions are obtained as [Atluri (2004)]

$$\phi^a_{,k} = \sum_{j=1}^{m} \left[p^j_{,k}(\mathbf{A}^{-1}\mathbf{B})^{ja} + p^j(\mathbf{A}^{-1}\mathbf{B}_{,k} + \mathbf{A}^{-1}_{,k}\mathbf{B})^{ja}\right], \tag{10}$$

wherein $\mathbf{A}^{-1}_{,k} = \left(\mathbf{A}^{-1}\right)_{,k}$ represents the derivative of the inverse of $\mathbf{A}$ with respect to x_k, given by

$$\mathbf{A}^{-1}_{,k} = -\mathbf{A}^{-1}\mathbf{A}_{,k}\mathbf{A}^{-1}.$$

3 Meshless local integral equations for heat conduction problems in shallow shells

Because of the present use of an uncoupled thermo-elastic theory, the thermal problem should

be solved first, in order to determine the temperature distribution within the shell in solving the shell problem under thermal loading. Material properties are assumed to be continuously variable along the shell thickness. Therefore, we shall consider a boundary value problem for the heat conduction problem in a continuously nonhomogeneous anisotropic medium, which is described by the governing equation:

$$\rho(\mathbf{x})c(\mathbf{x})\frac{\partial\theta}{\partial t}(\mathbf{x},t)=\left[\lambda_{ij}(\mathbf{x})\theta_{,j}(\mathbf{x},t)\right]_{,i}+Q(\mathbf{x},t) \tag{11}$$

where $\theta(\mathbf{x},t)$ is the temperature field, $Q(\mathbf{x},t)$ is the density of body heat sources, λ_{ij} is the thermal conductivity tensor, $\rho(\mathbf{x})$ is the mass density and $c(\mathbf{x})$ the specific heat.

Let the analyzed domain of the shallow shell is denoted by Ω with the top and bottom surfaces being S^+ and S^-, respectively. Arbitrary temperature or heat flux boundary conditions can be prescribed on all considered surfaces. The initial condition is assumed

$$\theta(\mathbf{x},t)|_{t=0}=\theta(\mathbf{x},0)$$

in the analyzed domain Ω.

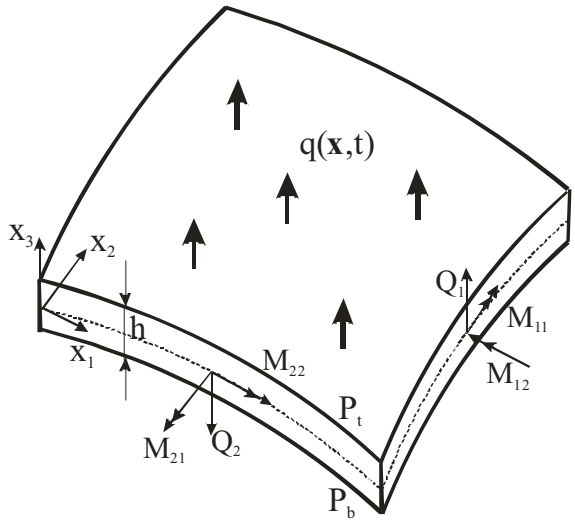

Figure 2: Sign convention of bending moments and forces for FGM shallow shell

A similar problem for a plate has been recently solved by Qian and Batra (2005) by an approximate computational technique. In their approach, the temperature field is expanded in the plate thickness direction by using Legendre polynomials as basis functions. The original 3-D problem is transformed into a set of 2-D problems there. In the present paper, a more general 3-D analysis based on the MLPG method is applied. The MLS approximation is used here. The approximations described in Sect. 2 for 2-D problems are still valid with only a modification of basis polynomials as

$$\begin{aligned}\mathbf{p}^T(\mathbf{x})&=[1,\,x_1,\,x_2,\,x_3],\quad \text{linear basis } m=4\\ \mathbf{p}^T(\mathbf{x})&=\big[1,\,x_1,\,x_2,\,x_3,\,(x_1)^2,\,(x_2)^2,\,(x_3)^2,\\ &\quad x_1x_2,\,x_3x_2,\,x_1x_3,\,(x_1)^2x_3,\,(x_2)^2x_3,\,(x_3)^2x_1\big]\\ &\qquad\text{quadratic basis } m=10.\end{aligned} \tag{12}$$

Applying the Laplace transformation to the governing equation (11), one obtains

$$\left[\lambda_{ij}(\mathbf{x})\overline{\theta}_{,j}(\mathbf{x},s)\right]_{,i}-\rho(\mathbf{x})c(\mathbf{x})s\overline{\theta}(\mathbf{x},s)=-\overline{F}(\mathbf{x},s) \tag{13}$$

where

$$\overline{F}(\mathbf{x},s)=\overline{Q}(\mathbf{x},s)+\theta(\mathbf{x},0)$$

is the redefined body heat source in the Laplace transform domain, with the inclusion of the initial boundary condition for the temperature and s is the Laplace transform parameter.

Again the weak form is constructed over local subdomains Ω_s, which is a small sphere taken for each node inside the global domain. The local weak form of the governing equation (13) for $\mathbf{x}^a\in\Omega_s^a$ can be written as

$$\int_{\Omega_s^a}\Big[\left(\lambda_{lj}(\mathbf{x})\overline{\theta}_{,j}(\mathbf{x},s)\right)_{,l}-\rho(\mathbf{x})c(\mathbf{x})s\overline{\theta}(\mathbf{x},s)+\overline{F}(\mathbf{x},s)\Big]\theta^*(\mathbf{x})d\Omega=0 \tag{14}$$

where $\theta^*(\mathbf{x})$ is a weight (test) function.

Applying the Gauss divergence theorem to equa-

tion (14), we obtain

$$\int_{\partial\Omega_s^a} \overline{q}(\mathbf{x},s)\theta^*(\mathbf{x})d\Gamma - \int_{\Omega_s^a} \lambda_{lj}(\mathbf{x})\overline{\theta}_{,j}(\mathbf{x},s)\theta^*_{,l}(\mathbf{x})d\Omega - \int_{\Omega_s^a} \rho(\mathbf{x})c(\mathbf{x})s\overline{\theta}(\mathbf{x},s)\theta^*(\mathbf{x})d\Omega + \int_{\Omega_s^a} \overline{F}(\mathbf{x},s)\theta^*(\mathbf{x})d\Omega = 0, \quad (15)$$

where $\partial\Omega_s^a$ is the boundary of the local subdomain and

$$\overline{q}(\mathbf{x},s) = \lambda_{lj}(\mathbf{x})\overline{\theta}_{,j}(\mathbf{x},s)n_l(\mathbf{x}).$$

The local weak form (15) is a starting point to derive local boundary integral equations providing an appropriate test function selection. If a Heaviside step function is chosen as the test function $\theta^*(\mathbf{x})$ in each subdomain

$$\theta^*(\mathbf{x}) = \begin{cases} 1 & \text{at } \mathbf{x} \in \Omega_s^a \\ 0 & \text{at } \mathbf{x} \notin \Omega_s^a \end{cases}$$

the local weak form (15) is transformed into the following simple local boundary integral equation

$$\int_{\partial\Omega_s^a} \overline{q}(\mathbf{x},s)d\Gamma - \int_{\Omega_s^a} \rho(\mathbf{x})c(\mathbf{x})s\overline{\theta}(\mathbf{x},s)d\Omega = -\int_{\Omega_s^a} \overline{F}(\mathbf{x},s)d\Omega. \quad (16)$$

Equation (16) is recognized as the balance of thermal energy on the subdomain Ω_s^a. In the stationary case, the domain integral on the left hand side of this local boundary integral equation vanishes. Finally, assuming vanishing heat sources and initial condition, we arrive at a pure boundary integral formulation.

The MLS approximation of the heat flux $\overline{q}(\mathbf{x},s)$ is assumed as

$$\overline{q}^h(\mathbf{x},s) = \lambda_{ij}n_i \sum_{a=1}^{n} \phi^a_{,j}(\mathbf{x})\hat{\theta}^a(s).$$

Substituting the MLS-approximations into the local integral equation (16), the system of algebraic equations is obtained

$$\sum_{a=1}^{n} \left(\int_{L_s+\Gamma_{sp}} \mathbf{n}^T \Lambda \mathbf{P}^a(\mathbf{x})d\Gamma - \int_{\Omega_s} \rho cs\phi^a(\mathbf{x})d\Gamma \right) \hat{\theta}^a(s) = -\int_{\Gamma_{sq}} \tilde{\overline{q}}(\mathbf{x},s)d\Gamma - \int_{\Omega_s} \overline{F}(\mathbf{x},s)d\Omega \quad (17)$$

at interior nodes as well as at the boundary nodes on $\partial\Omega_N$, where $\partial\Omega_N$ is the part of the global boundary surface $\partial\Omega$ on which the heat flux is prescribed and $\Gamma_{sq} = \partial\Omega_s \cap \partial\Omega_N$. In equation (17), we have used the notations

$$\Lambda = \begin{bmatrix} \lambda_{11} & \lambda_{12} & \lambda_{13} \\ \lambda_{12} & \lambda_{22} & \lambda_{23} \\ \lambda_{13} & \lambda_{23} & \lambda_{33} \end{bmatrix}, \quad \mathbf{P}^a(\mathbf{x}) = \begin{bmatrix} \phi^a_{,1} \\ \phi^a_{,2} \\ \phi^a_{,3} \end{bmatrix},$$
$$\mathbf{n}^T = (n_1, n_2, n_3),$$
$$L_s \cup \Gamma_{sp} = \partial\Omega_s, \quad \Gamma_{sp} = \partial\Omega_s \cap \partial\Omega_D, \quad \partial\Omega = \partial\Omega_D \cup \partial\Omega_N. \quad (18)$$

The time dependent values of the transformed quantities can be obtained by an inverse Laplace-transformation. In the present analysis, the Stehfest's inversion algorithm [Stehfest (1970)] is used.

4 Analyses of orthotropic FGM shallow shells under a thermal load

Consider a linear elastic orthotropic shallow shell of constant thickness h and with its mid-surface being described by $x_3 = f(x_1,x_2)$ in a domain S with the boundary contour Γ in the base plane $x_1 - x_2$. The Reissner-Mindlin bending theory [Reissner (1946)] is used to describe the shell deformation. The total displacements of the shell are given by the superposition of the bending deformations and the membrane deformations. Then, the spatial displacement field u'_i and strains ε'_{ij} caused by bending are the same as for a plate and they are given by [Reddy (1997)]

$$u'_1(\mathbf{x},t) = x_3 w_1(\mathbf{x},t),$$
$$u'_2(\mathbf{x},t) = x_3 w_2(\mathbf{x},t),$$
$$u'_3(\mathbf{x},t) = w_3(\mathbf{x},t), \quad (19)$$

where w_α and w_3 represent the rotations around the x_α-direction and the out-of-plane deflection, respectively (see Fig. 2). The corresponding linear strains are given by

$$\begin{aligned}
\varepsilon'_{11}(\mathbf{x},t) &= x_3 w_{1,1}(\mathbf{x},t),\\
\varepsilon'_{22}(\mathbf{x},t) &= x_3 w_{2,2}(\mathbf{x},t),\\
\varepsilon'_{12}(\mathbf{x},t) &= x_3 (w_{1,2}(\mathbf{x},t) + w_{2,1}(\mathbf{x},t))/2,\\
\varepsilon'_{13}(\mathbf{x},t) &= (w_1(\mathbf{x},t) + w_{3,1}(\mathbf{x},t))/2,\\
\varepsilon'_{23}(\mathbf{x},t) &= (w_2(\mathbf{x},t) + w_{3,2}(\mathbf{x},t))/2.
\end{aligned} \tag{20}$$

Since $\varepsilon'_{33} = 0$, we have on the mid-surface $\sigma'_{33} = 0$. Assuming $\sigma'_{33} = 0$ throughout the shell thickness, one can write the constitutive equations for orthotropic materials as

$$\begin{bmatrix} \sigma'_{11} \\ \sigma'_{22} \\ \sigma'_{12} \\ \sigma'_{13} \\ \sigma'_{23} \end{bmatrix} = \mathbf{D}'(\mathbf{x}) \begin{bmatrix} \varepsilon'_{11} \\ \varepsilon'_{22} \\ 2\varepsilon'_{12} \\ 2\varepsilon'_{13} \\ 2\varepsilon'_{23} \end{bmatrix}, \tag{21}$$

where

$$\mathbf{D}'(\mathbf{x}) = \begin{bmatrix} E_1/e & E_2\nu_{12}/e & 0 & 0 & 0 \\ E_2\nu_{12}/e & E_2/e & 0 & 0 & 0 \\ 0 & 0 & G_{12} & 0 & 0 \\ 0 & 0 & 0 & G_{13} & 0 \\ 0 & 0 & 0 & 0 & G_{23} \end{bmatrix}$$

with $e = 1 - \nu_{12}\nu_{21}$.

Here, E_k are Young's moduli referred to the axes x_k (k=1, 2), G_{12}, $G_{13}$and G_{23} are the shear moduli, and ν_{ij} are Poisson's ratios.

The membrane strains have the form [Lukasiewicz (1979)]

$$\varepsilon_{\alpha\beta} = \frac{1}{2}(u_{\alpha,\beta} + u_{\beta,\alpha}) + \delta_{\alpha\beta} k_{\alpha\beta} w_3, \tag{22}$$

where $k_{\alpha\beta}$ are the principal curvatures of the shell in x_1- and x_2-directions with the assumption $k_{12} = k_{21} = 0$, and u_α are the in-plane displacements. The summation convention is not assumed in Eq. (22).

Then, the membrane stresses are given as

$$\begin{bmatrix} \sigma_{11} \\ \sigma_{22} \\ \sigma_{12} \end{bmatrix} = \mathbf{D}(\mathbf{x}) \begin{bmatrix} \varepsilon_{11} \\ \varepsilon_{22} \\ 2\varepsilon_{12} \end{bmatrix} - \begin{bmatrix} \gamma_{11} \\ \gamma_{22} \\ 0 \end{bmatrix} \theta(x_1, x_2, 0, t),$$

(23)

where

$$\mathbf{D}(\mathbf{x}) = \begin{bmatrix} E_1/e & E_1\nu_{21}/e & 0 \\ E_2\nu_{12}/e & E_2/e & 0 \\ 0 & 0 & G_{12} \end{bmatrix}.$$

Next, we assume that the material properties are graded along the shell thickness, and the profile of the volume fraction variation is described by

$$P(x_3) = P_b + (P_t - P_b)V_f \text{ with } V_f = \left(\frac{x_3}{h} + \frac{1}{2}\right)^n, \tag{24}$$

where P denotes a generic property like Young's or shear modulus, P_t and P_b denote the property of the top and the bottom faces of the shell, respectively, and n is a parameter that controls the material variation profile (see Fig. 3). Poisson's ratios are assumed to be constant.

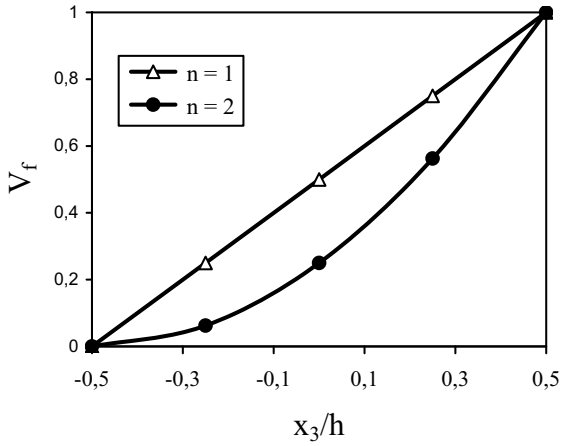

Figure 3: Variation of the volume fraction over the shell thickness for linear and quadratic power-law index

The bending moments $M_{\alpha\beta}$, the shear forces Q_α and the normal forces $N_{\alpha\beta}$ are defined as

$$\begin{bmatrix} M_{11} \\ M_{22} \\ M_{12} \end{bmatrix} = \int_{-h/2}^{h/2} \begin{bmatrix} \sigma'_{11} \\ \sigma'_{22} \\ \sigma'_{12} \end{bmatrix} x_3 dx_3,$$

$$\begin{bmatrix} Q_1 \\ Q_2 \end{bmatrix} = \kappa \int_{-h/2}^{h/2} \begin{bmatrix} \sigma'_{13} \\ \sigma'_{23} \end{bmatrix} dx_3,$$

$$\begin{bmatrix} N_{11} \\ N_{22} \\ N_{12} \end{bmatrix} = \int_{-h/2}^{h/2} \begin{bmatrix} \sigma_{11} \\ \sigma_{22} \\ \sigma_{12} \end{bmatrix} dx_3, \tag{25}$$

where $\kappa = 5/6$ in the Reissner plate theory.

Substituting equations (20) and (21) into moment and force resultants (25) allows the expression of the bending moments $M_{\alpha\beta}$ and shear forces Q_α for α, β=1,2, in terms of rotations, lateral displacements of the orthotropic plate and temperature. In the case of considered continuous gradation of material properties through the plate thickness, one obtains

$$\begin{aligned} M_{\alpha\beta} &= D_{\alpha\beta}\left(w_{\alpha,\beta} + w_{\beta,\alpha}\right) + C_{\alpha\beta} w_{\gamma,\gamma} - H_{\alpha\beta} \\ Q_\alpha &= C_\alpha \left(w_\alpha + w_{3,\alpha}\right), \end{aligned} \tag{26}$$

where

$$H_{\alpha\beta} = \int_{-h/2}^{h/2} x_3 \gamma_{\alpha\beta} \theta(\mathbf{x}, x_3, t) dx_3.$$

In eq. (26), repeated indices α, β do not imply summation, and the material parameters $D_{\alpha\beta}$ and $C_{\alpha\beta}$ are given as

$$\begin{aligned} &D_{11} = \frac{D_1}{2}(1-\nu_{21}), \quad D_{22} = \frac{D_2}{2}(1-\nu_{12}), \\ &D_{12} = D_{21} = \frac{\overline{G}_{12} h^3}{12}, \\ &C_{11} = D_1 \nu_{21}, \quad C_{22} = D_2 \nu_{12}, \quad C_{12} = C_{21} = 0, \\ &D_\alpha = \frac{\overline{E}_\alpha h^3}{12e}, \quad D_1 \nu_{21} = D_2 \nu_{12}, \quad C_\alpha = \kappa h \overline{G}_{\alpha 3}, \end{aligned} \tag{27}$$

where

$$\overline{E}_\alpha \equiv \begin{cases} E_{\alpha t} = E_{\alpha b}, n = 0 \\ (E_{\alpha b} + E_{\alpha t})/2, n = 1 \\ (3E_{\alpha b} + 2E_{\alpha t})/5, n = 2 \end{cases}$$

$$\overline{G}_{12} \equiv \begin{cases} G_{12t} = G_{12b}, n = 0 \\ (G_{12b} + G_{12t})/2, n = 1 \\ (3G_{12b} + 2G_{12t})/5, n = 2 \end{cases},$$

$$\overline{G}_{\alpha 3} \equiv \begin{cases} G_{\alpha 3t} = G_{\alpha 3b}, n = 0 \\ (G_{\alpha 3b} + G_{\alpha 3t})/2, n = 1 \\ (2G_{\alpha 3b} + G_{\alpha 3t})/3, n = 2 \end{cases},$$

with the same meaning of subscripts b and t as in Eq. (24).

For a general variation of material properties through the shell thickness:

$$\begin{aligned} D_{11} &= \int_{-h/2}^{h/2} x_3^2 E_1(x_3) \frac{1-\nu_{21}}{e} dx_3, \\ D_{22} &= \int_{-h/2}^{h/2} x_3^2 E_2(x_3) \frac{1-\nu_{12}}{e} dx_3, \\ D_{12} &= \int_{-h/2}^{h/2} x_3^2 G_{12}(x_3) dx_3, \\ C_{11} &= \int_{-h/2}^{h/2} x_3^2 E_1(x_3) \frac{\nu_{21}}{e} dx_3, \\ C_{22} &= \int_{-h/2}^{h/2} x_3^2 E_2(x_3) \frac{\nu_{12}}{e} dx_3, \\ C_\alpha &= \kappa \int_{-h/2}^{h/2} G_{\alpha 3}(x_3) dx_3. \end{aligned}$$

Similarly substituting Eqs. (22) and (23) into the force resultants (25) one obtains the expression of the normal forces $N_{\alpha\beta}$ (α, β=1, 2) in terms of the deflection and the lateral displacements of the orthotropic shell

$$\begin{bmatrix} N_{11} \\ N_{22} \\ N_{12} \end{bmatrix} = \mathbf{P} \begin{bmatrix} u_{1,1} \\ u_{2,2} \\ u_{1,2} + u_{2,1} \end{bmatrix} + \begin{bmatrix} Q_{11} \\ Q_{22} \\ 0 \end{bmatrix} w_3 - \begin{bmatrix} \theta_{11} \\ \theta_{22} \\ 0 \end{bmatrix}, \tag{28}$$

where

$$\begin{aligned} \theta_{\alpha\beta} &= \int_{-h/2}^{h/2} \gamma_{\alpha\beta} \theta(\mathbf{x}, x_3, t) dx_3, \\ \mathbf{P} &= \begin{bmatrix} E_1^*/e & E_1^* \nu_{12}/e & 0 \\ E_2^* \nu_{12}/e & E_2^*/e & 0 \\ 0 & 0 & G_{12}^* \end{bmatrix}, \\ \begin{bmatrix} Q_{11} \\ Q_{22} \\ 0 \end{bmatrix} &= \begin{bmatrix} (k_{11} + k_{22}\nu_{12}) E_1^*/e \\ (k_{11}\nu_{12} + k_{22}) E_2^*/e \\ 0 \end{bmatrix}, \end{aligned} \tag{29}$$

$$E_\alpha^* \equiv \int_{-\frac{h}{2}}^{\frac{h}{2}} E_\alpha(x_3) dx_3 = \begin{cases} E_{\alpha t} = E_{\alpha b}, & n = 0 \\ \frac{E_{\alpha b} + E_{\alpha t}}{2}, & n = 1 \\ \frac{2E_{\alpha b} + E_{\alpha t}}{3}, & n = 2 \end{cases},$$

$$G_{12}^{*} \equiv \int_{-\frac{h}{2}}^{\frac{h}{2}} G_{12}(x_3)dx_3 = \begin{cases} G_{12t} = G_{12b}, & n=0 \\ \frac{G_{12b}+G_{12t}}{2}, & n=1 \\ \frac{2G_{12b}+G_{12t}}{3}, & n=2 \end{cases}.$$

Using the Reissner's linear theory of shallow shells [Reissner (1946)], the quasi-static form of the equations of motion may be written as

$$\begin{aligned} &M_{\alpha\beta,\beta}(\mathbf{x},t) - Q_{\alpha}(\mathbf{x},t) = 0, \\ &Q_{\alpha,\alpha}(\mathbf{x},t) - k_{\alpha\beta}N_{\alpha\beta}(\mathbf{x},t) = 0, \\ &N_{\alpha\beta,\beta}(\mathbf{x},t) = 0, \quad \mathbf{x} \in S. \end{aligned} \tag{30}$$

Thermal changes in solids are relatively slow with respect to elastic wave velocity. Therefore, inertial terms are not considered in governing equations. Moreover, mechanical loads are considered to be vanishing too. The problem of a shell under a mechanical load has been analyzed recently by authors [Sladek et al. (2008a)].

The MLPG method constructs the weak-form over local subdomains S_s

$$\int_{\Omega_s^i} \left[M_{\alpha\beta,\beta}(\mathbf{x},t) - Q_{\alpha}(\mathbf{x},t)\right] w_{\alpha\gamma}^{*}(\mathbf{x})d\Omega = 0, \tag{31}$$

$$\int_{\Omega_s^i} \left[Q_{\alpha,\alpha}(\mathbf{x},t) - k_{\alpha\beta}N_{\alpha\beta}(\mathbf{x},t)\right] w_3^{*}(\mathbf{x})d\Omega = 0, \tag{32}$$

$$\int_{\Omega_s^i} \left[N_{\alpha\beta,\beta}(\mathbf{x},t)\right] u_{\alpha\gamma}^{*}(\mathbf{x})d\Omega = 0. \tag{33}$$

Applying the Gauss divergence theorem to local weak forms and choosing the test functions as a unit step function with support in the current subdomain

$$w_{\alpha\gamma}^{*}(\mathbf{x}) = \begin{cases} \delta_{\alpha\gamma}, & \text{at } \mathbf{x} \in (S_s \cup \partial S_s) \\ 0, & \text{at } \mathbf{x} \notin (S_s \cup \partial S_s) \end{cases},$$

$$w^{*}(\mathbf{x}) = \begin{cases} 1, & \text{at } \mathbf{x} \in (S_s \cup \partial S_s) \\ 0, & \text{at } \mathbf{x} \notin (S_s \cup \partial S_s) \end{cases}$$

one obtains local boundary-domain integral equations

$$\int_{\partial S_s^i} M_{\alpha}(\mathbf{x},t)d\Gamma - \int_{S_s^i} Q_{\alpha}(\mathbf{x},t)d\Omega = 0 \tag{34}$$

$$\int_{\partial S_s^i} Q_{\alpha}(\mathbf{x},t)n_{\alpha}(\mathbf{x})d\Gamma - \int_{S_s^i} k_{\alpha\beta}(\mathbf{x})N_{\alpha\beta}(\mathbf{x},t)d\Omega = 0 \tag{35}$$

$$\int_{\partial S_s^i} T_{\alpha}(\mathbf{x},t)d\Gamma = 0. \tag{36}$$

where

$$T_{\alpha}(\mathbf{x},t) = N_{\alpha\beta}(\mathbf{x},t)n_{\beta}(\mathbf{x}). \tag{37}$$

According to Sect.2, one can write the approximation formula for the generalized displacements (two rotations and deflection) as

$$\mathbf{w}^{h}(\mathbf{x},t) = \mathbf{\Phi}^{T}(\mathbf{x}) \cdot \hat{\mathbf{w}}(t) = \sum_{a=1}^{n} \phi^{a}(\mathbf{x})\hat{\mathbf{w}}^{a}(t), \tag{38}$$

Substituting the approximation (38) into the definition of the normal bending (26), one obtains for $\mathbf{M}(\mathbf{x},t) = [M_1(\mathbf{x},t), M_2(\mathbf{x},t)]^{T}$

$$\begin{aligned} \mathbf{M}(\mathbf{x},t) &= \mathbf{N_1} \sum_{a=1}^{n} \mathbf{B}_1^{a}(\mathbf{x})\mathbf{w}^{*a}(t) + \mathbf{N_2} \sum_{a=1}^{n} \mathbf{B}_2^{a}(\mathbf{x})\mathbf{w}^{*a}(t) \\ &\quad - \mathbf{H}(\mathbf{x},t) \\ &= \mathbf{N}_{\alpha}(\mathbf{x}) \sum_{a=1}^{n} \mathbf{B}_{\alpha}^{a}(\mathbf{x})\mathbf{w}^{*a}(t) - \mathbf{H}(\mathbf{x},t), \end{aligned} \tag{39}$$

where the vector $\mathbf{w}^{*a}(t)$ is defined as a column vector $\mathbf{w}^{*a}(t) = [\hat{w}_1^{a}(t), \hat{w}_2^{a}(t)]^{T}$, the vector $\mathbf{H}(\mathbf{x},t) = [H_{11}n_1, H_{22}n_2]^{T}$, the matrices $\mathbf{N}_{\alpha}(\mathbf{x})$ are related to the normal vector **n(x)** on ∂S_s by

$$\mathbf{N}_1(\mathbf{x}) = \begin{bmatrix} n_1 & 0 & n_2 \\ 0 & n_2 & n_1 \end{bmatrix}$$

and

$$\mathbf{N}_2(\mathbf{x}) = \begin{bmatrix} C_{11} & 0 \\ 0 & C_{22} \end{bmatrix} \begin{bmatrix} n_1 & n_1 \\ n_2 & n_2 \end{bmatrix}$$

and the matrices $\mathbf{B}_{\alpha}^{a}$ are represented by the gradients of the shape functions as

$$\mathbf{B}_1^{a}(\mathbf{x}) = \left[\begin{bmatrix} 2D_{11}\phi_{,1}^{a} \\ 0 \\ D_{12}\phi_{,2}^{a} \end{bmatrix} \quad \begin{bmatrix} 0 \\ 2D_{22}\phi_{,2}^{a} \\ D_{12}\phi_{,1}^{a} \end{bmatrix} \right],$$

$$\mathbf{B}_2^{a}(\mathbf{x}) = \begin{bmatrix} \phi_{,1}^{a} & 0 \\ 0 & \phi_{,2}^{a} \end{bmatrix}.$$

The influence on the material gradation is incorporated in $C_{\alpha\beta}$ and $D_{\alpha\beta}$ defined in equation (27). Similarly one can obtain the approximation for the shear forces

$$\mathbf{Q}(\mathbf{x},t) = \mathbf{C}(\mathbf{x}) \sum_{a=1}^{n} [\phi^a(\mathbf{x})\mathbf{w}^{*a}(t) + \mathbf{F}^a(\mathbf{x})\hat{w}_3^a(t)], \tag{40}$$

where $\mathbf{Q}(\mathbf{x},t) = [Q_1(\mathbf{x},t), Q_2(\mathbf{x},t)]^T$ and

$$\mathbf{C}(\mathbf{x}) = \begin{bmatrix} C_1(\mathbf{x}) & 0 \\ 0 & C_2(\mathbf{x}) \end{bmatrix}, \quad \mathbf{F}^a(\mathbf{x}) = \begin{bmatrix} \phi^a_{,1} \\ \phi^a_{,2} \end{bmatrix}.$$

Then,

$$n_\alpha(\mathbf{x})Q_\alpha(\mathbf{x},t) = \mathbf{C}_n(\mathbf{x}) \sum_{a=1}^{n} [\phi^a(\mathbf{x})\mathbf{w}^{*a}(t) + \mathbf{F}^a(\mathbf{x})\hat{w}_3^a(t)]$$

with

$$\mathbf{C}_n(\mathbf{x}) = \begin{bmatrix} n_1(\mathbf{x})C_1(\mathbf{x}), & n_2(\mathbf{x})C_2(\mathbf{x}) \end{bmatrix}.$$

The in-plane displacements are approximated by

$$\mathbf{u}^h(\mathbf{x},t) = \Phi^T(\mathbf{x}) \cdot \hat{\mathbf{u}}(t) = \sum_{a=1}^{n} \phi^a(\mathbf{x})\hat{\mathbf{u}}^a(t). \tag{41}$$

Then, the traction vector can be expressed as

$$T(\mathbf{x},t) = \mathbf{N}_1(\mathbf{x})\mathbf{P}(\mathbf{x}) \sum_{a=1}^{n} \mathbf{B}^a(\mathbf{x})\mathbf{u}^{*a}(t) + \mathbf{J}(\mathbf{x}) \sum_{a=1}^{n} \phi^a(\mathbf{x})\hat{w}_3^a(t) - \Theta(\mathbf{x},t), \tag{42}$$

where the vector $\mathbf{u}^{*a}(t)$ is defined as a column vector $\mathbf{u}^{*a}(t) = [\hat{u}_1^a(t),\ \hat{u}_2^a(t)]^{\mathrm{T}}$, $\Theta(\mathbf{x},t) = [\theta_{11}n_1,\ \theta_{22}n_2]^T$, $\mathbf{J}(\mathbf{x}) = [Q_{11}n_1,\ Q_{22}n_2]^T$,

$$\mathbf{B}^a(\mathbf{x}) = \begin{bmatrix} \begin{bmatrix} \phi^a_{,1} \\ 0 \\ \phi^a_{,2} \end{bmatrix} & \begin{bmatrix} 0 \\ \phi^a_{,2} \\ \phi^a_{,1} \end{bmatrix} \end{bmatrix}.$$

We need to approximate also

$$k_{\alpha\beta}(\mathbf{x})N_{\alpha\beta}(\mathbf{x},t) = \mathbf{K}(\mathbf{x})^{\mathrm{T}}\mathbf{P}(\mathbf{x}) \sum_{a=1}^{n} \mathbf{B}^a(\mathbf{x})\mathbf{u}^{*a}(t) + O(\mathbf{x}) \sum_{a=1}^{n} \phi^a(\mathbf{x})\hat{w}_3^a(t) - \theta_{11}(\mathbf{x})k_{11}(\mathbf{x}) + \theta_{22}(\mathbf{x})k_{22}(\mathbf{x}), \tag{43}$$

where

$$\mathbf{K}(\mathbf{x}) = \begin{bmatrix} k_{11} \\ k_{22} \\ 2k_{12} \end{bmatrix},$$

$$O(\mathbf{x}) = Q_{11}(\mathbf{x})k_{11}(\mathbf{x}) + Q_{22}(\mathbf{x})k_{22}(\mathbf{x}).$$

Furthermore, in view of the MLS approximations (39), (40) and (42) for the unknown fields in the local boundary-domain integral equations (34) - (36), we obtain their discretized forms as

$$\sum_{a=1}^{n} \left[\int_{L_s^i + \Gamma_{sw}^i} \mathbf{N}_\alpha(\mathbf{x})\mathbf{B}_\alpha^a(\mathbf{x})d\Gamma - \int_{S_s^i} \mathbf{C}(\mathbf{x})\phi^a(\mathbf{x})d\Omega \right] \mathbf{w}^{*a}(t) - \sum_{a=1}^{n} \left[\int_{S_s^i} \mathbf{C}(\mathbf{x})\mathbf{F}^a(\mathbf{x})d\Omega \right] \hat{w}_3^a(t) = \int_{L_s^i + \Gamma_{sM}^i} \mathbf{H}(\mathbf{x},t)d\Gamma - \int_{\Gamma_{sM}^i} \tilde{\mathbf{M}}(\mathbf{x},t)d\Gamma \tag{44}$$

$$\sum_{a=1}^{n} \left[\int_{\partial S_s^i} \mathbf{C}_n(\mathbf{x})\phi^a(\mathbf{x})d\Gamma \right] \mathbf{w}^{*a}(t) - \mathbf{K}(\mathbf{x})^{\mathrm{T}}\mathbf{P}(\mathbf{x}) \sum_{a=1}^{n} \left[\int_{S_s^i} \mathbf{B}^a(\mathbf{x})d\Omega \right] \mathbf{u}^{*a}(t) + \sum_{a=1}^{n} \left[\int_{\partial S_s^i} \mathbf{C}_n(\mathbf{x})\mathbf{F}^a(\mathbf{x})d\Gamma - \int_{S_s^i} O(\mathbf{x})\phi^a(\mathbf{x})d\Omega \right] \hat{w}_3^a(t) = \int_{S_s^i} [\theta_{11}(\mathbf{x},t)k_{11} + \theta_{22}(\mathbf{x},t)k_{22}]\, d\Omega \tag{45}$$

$$\sum_{a=1}^{n} \left[\int_{L_s^i + \Gamma_{su}^i} \mathbf{N}_1(\mathbf{x})\mathbf{P}(\mathbf{x})\mathbf{B}^a(\mathbf{x})d\Gamma \right] \mathbf{u}^{*a}(t) + \sum_{a=1}^{n} \left[\int_{S_s^i} \mathbf{J}(\mathbf{x})\phi^a(\mathbf{x})d\Omega \right] \hat{w}_3^a(t) = \int_{L_s^i + \Gamma_{sM}^i} \Theta(\mathbf{x},t)d\Gamma - \int_{\Gamma_{sP}^i} \tilde{\mathbf{T}}(\mathbf{x},t)d\Gamma. \tag{46}$$

Recall that the discretized local boundary-domain integral equations (44)-(46) are considered on the sub-domains adjacent to the interior nodes $\mathbf{x}^i$ as well as to the boundary nodes on Γ^i_{sM} and Γ^i_{sP}. For the source point $\mathbf{x}^i$ located on the global boundary Γ the boundary of the subdomain ∂S^i_s is composed of the interior and the boundary portions L^i_s and Γ^i_{sM}, respectively, or alternatively of L^i_s and Γ^i_{sP}, with the portions Γ^i_{sM} and Γ^i_{sP} lying on the global boundary with prescribed bending moments or stress vector, respectively. Equations (44) and (46) are vector equations for the two components of rotations and in-plane displacements, respectively. Then, the set of Eqs. (44)–(46) represents 5 equations at each node for five unknown components, namely, two rotations, one out-of-plane deflection and two in-plane displacements.

It should be noted here that there are neither Lagrange-multipliers nor penalty parameters introduced into the local weak-forms (31) - (33) because the essential boundary conditions on Γ^i_{sw} or Γ^i_{su} can be imposed directly by using the MLS approximations (38) and (41)

$$\sum_{a=1}^{n} \phi^a(\mathbf{x})\hat{\mathbf{w}}^a(t) = \tilde{\mathbf{w}}(\mathbf{x}^i,t) \text{ for } \mathbf{x}^i \in \Gamma^i_{sw} = \Gamma_w \cap (S^i_s \cup \partial S^i_s), \quad (47)$$

$$\sum_{a=1}^{n} \phi^a(\mathbf{x})\hat{\mathbf{u}}^a(t) = \tilde{\mathbf{u}}(\mathbf{x}^i,t) \text{ for } \mathbf{x}^i \in \Gamma^i_{su} = \Gamma_u \cap (S^i_s \cup \partial S^i_s), \quad (48)$$

where $\tilde{\mathbf{w}}(\mathbf{x}^i,t) = \left[\tilde{w}_1(\mathbf{x}^i,t), \tilde{w}_2(\mathbf{x}^i,t), \tilde{w}_3(\mathbf{x}^i,t)\right]^T$ are the prescribed values of two rotations and the deflection at the nodal point $\mathbf{x}^i$ on the portion of the global boundary, Γ_w, while $\tilde{\mathbf{u}}(\mathbf{x}^i,t) = \left[\tilde{u}_1(\mathbf{x}^i,t), \quad \tilde{u}_2(\mathbf{x}^i,t)\right]^T$ are the prescribed values of in-plane displacements at the nodal point $\mathbf{x}^i$ on the portion of the global boundary Γ_u. The MLS approximation does not possess Kronecker-delta property in the present form. If a singular weight function were introduced into the MLS approximation, the Kronecker-delta property would be recovered [Chen and Wang (2000)]. In such a case instead of fictitious nodal values one would use the nodal values of the generalized displacements in the approximations (38) and (41) with assuming such nodal values being prescribed on Γ^i_{sw} and Γ^i_{su}, respectively. For essential boundary conditions only one column in the matrix form of Eq. (47) or (48) has prescribed quantities and other ones are zero. For a clamped shell all three vector components (two rotations and one deflection) and two components of the in-plane displacements are vanishing at the fixed edge and only Eqs. (47) and (48) are used at the boundary nodes in such a case. On the other hand, for a simply supported shell only the third component of the generalized displacement vector (i.e., the deflection) is prescribed and the rotations are unknown. Then, equations (44) and (46) together with Eq. (47) for the third vector component are applied for a point on the global boundary. If no geometrical boundary conditions are prescribed on the part of the boundary, all three local integral equations (44) - (46) are applied.

5 Numerical examples

A shallow spherical shell with a square contour is investigated in the first example here (see Fig. 4). We consider simply supported boundary conditions of the shell with a side-length $a = 0.254m$ and the thicknesses $h/a = 0.05$. On the top surface of the shell a uniformly distributed temperature $\theta = 1^0$ is considered. The bottom surface is kept at vanishing temperature. Stationary thermal conditions are assumed. In the first case homogeneous and isotropic medium is considered: Young's moduli $E_1 = E_2 = 0.6895 \cdot 10^{10}\text{N / m}^2$, Poisson's ratios $\nu_{21} = \nu_{12} = 0.3$, and the thermal expansion coefficients $\alpha_{11} = \alpha_{22} = 1 \cdot 10^{-5}\text{deg}^{-1}$. The used shear moduli correspond to Young's modulus E_2, namely, $G_{12} = G_{13} = G_{23} = E_2/2(1+\nu_{12})$.

The convergence study of the method is not presented here, since it was done for a similar plate problem [Sladek et al. (2008b)]. For the MLS approximation a regular node distribution with total 441 nodes is used here. The circular subdomain is chosen as $r_{loc} = 0.4s$ and the radius of the support domain for node a is$r^a = 4r_{loc}$, where s is a distance of two neighbouring nodes. Smaller values of the support domain lead to lower approximation accuracy, and larger values of the support do-

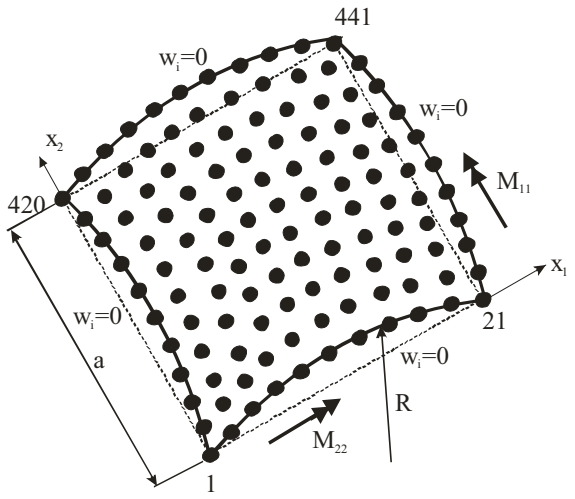

Figure 4: Geometry and boundary conditions of the square shallow spherical shell

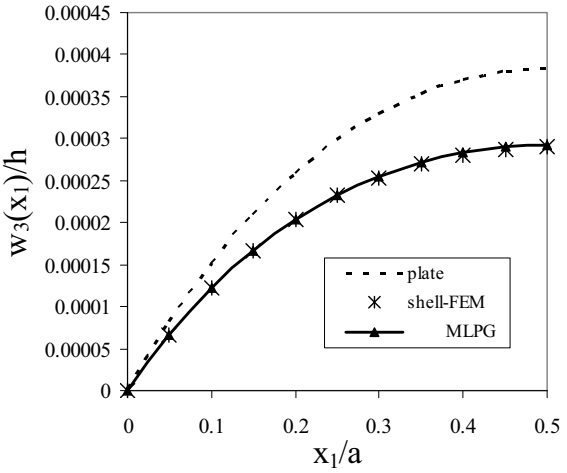

Figure 5: Variation of the deflection with thex_1-coordinate for a simply supported isotropic square shallow spherical shell with $R/a = 10$

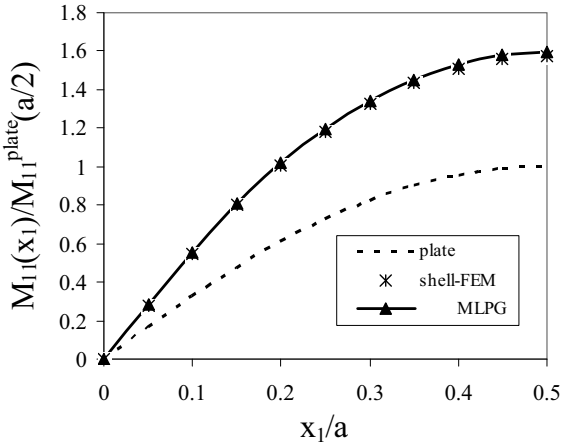

Figure 6: Variation of the bending moment with the x_1-coordinate for a simply supported isotropic square shallow spherical shell with $R/a = 10$

main prolong the computational time for the evaluation of the shape functions. The value of the radius of the support domain has been optimized on numerical experiments. Nie et al (2006) developed an efficient approach to find the optimal radius of support of radial weight functions used in MLS approximation.

The variation of the deflection with the x_1-coordinate at x_2= a/2 of the shell is presented in Fig. 5. The deflection is normalized to the shell thickness. The shell deflection with curvature $R/a = 10$ is compared with the deflection of the corresponding plate (i.e., curvature radius $R = \infty$) . The finite curvature of the shell reduces the deflection as compared with the plate case. One can observe a very good agreement of the present and analytical results. The FEM-ANSYS results have been obtained by using 400 quadrilateral eight-node elements.

The variation of the bending moment $M_{11}$is shown in Fig. 6. The bending moment is normalized by the central value for an isotropic plate, $M_{11}^{plate}(a/2) = 0.4634Nm$. The curvature of the shell has an opposite tendency on the bending moments as on deflections.

The thermal forces for the shell and corresponding plate are the same. However, the flexural rigidity of the shell is higher than for the corresponding plate. Then, the bending moment at the center of the shell has to be larger than the bending moment for the corresponding plate Again a very good agreement of the present and FEM results is observed.

Next, orthotropic mechanical properties of the shell are considered with Young's moduli $E_2 = 0.6895 \cdot 10^{10}\mathrm{N/m}^2$, $E_1 = 2E_2$, Poisson's ratios $\nu_{21} = 0.15$, $\nu_{12} = 0.3$. The variation of the deflection with the x_1-coordinate at $x_2 = a/2$ of the shell is presented in Fig. 7 with the assumption of

isotropic thermal expansion coefficients. Two different shell curvatures are considered here. Opposite to mechanical load case [Sladek et al. 2007b] the deflection is not reduced in the orthotropic plate as compared with the isotropic shell. It is due to increasing equivalent load for orthotropic plate at the same temperature distributions in both cases. The shell curvature has a strong influence on the shell deflection. The increasing curvature reduces the deflection. Numerical results obtained by the proposed method and FEM are compared for the shell curvature $R/a = 10$. It is observed again a very good agreement.

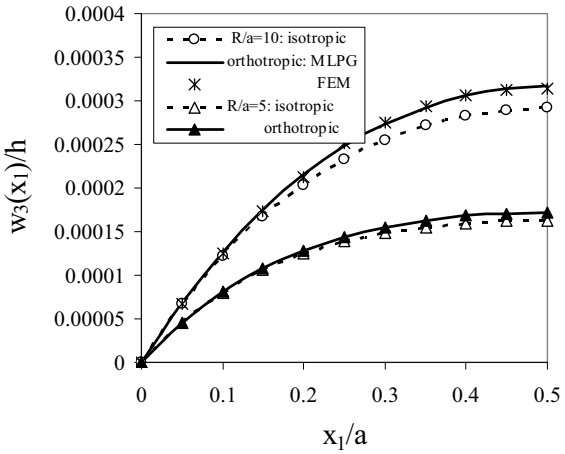

Figure 7: Influence of orthotropic material properties on the shell deflection

The variations of the bending moments M_{11} for orthotropic shells are presented in Fig. 8. We consider orthotropic properties for Young's moduli, while for the thermal expansion coefficients we assume isotropic behaviour. The bending moments are normalized by the central value for an isotropic plate, $M_{11}^{plate}(a/2) = 0.4634Nm$. One can observe that orthotropic material properties of mechanical coefficients have a strong influence on the bending moment values.

Next, functionally graded material properties through the shell thickness are considered. Both the isotropic and orthotropic properties are assumed as $E_{1t} = E_{2t} = 0.6895 \cdot 10^{10}\mathrm{N/m^2}$, Poisson's ratios $\nu_{12} = \nu_{21} = 0.3$ in the isotropic case, while $E_{2t} = 0.6895 \cdot 10^{10}\mathrm{N/m^2}$, $E_1 = 2E_2$, Poisson's ratios $\nu_{21} = 0.15$, $\nu_{12} = 0.3$ in the or-

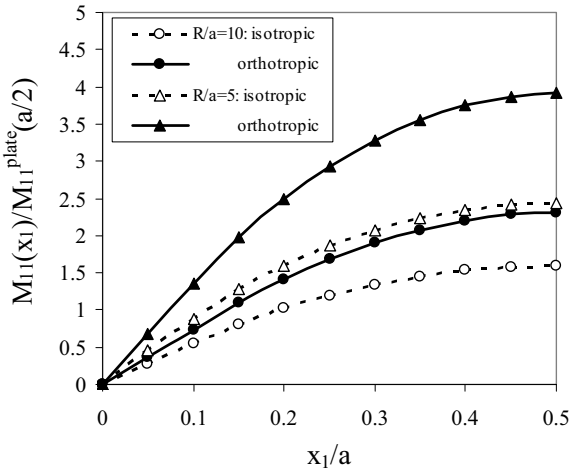

Figure 8: Variation of the bending moment with the x_1-coordinate for a simply supported orthotropic square shallow shell

thotropic case on top side of the shell. A quadratic variation of volume fraction V defined in equation (24) is considered here, and the Young's moduli on the bottom side are: $E_{1b} = E_{2b} = E_{2t}/2$ in the isotropic case, and $E_{1b}/2 = E_{2b} = E_{2t}/2$ in the orthotropic case. The variations of deflections with the x_1-coordinate are given in Fig. 9a and Fig. 9b for isotropic and orthotropic shell, respectively. Since Young's modulus on the bottom side is considered to be smaller than on the top one, the deflection for the FGM shell is larger than for the homogenenous shell with material properties corresponding to the top side, $E_{2t} = 0.6895 \cdot 10^{10}\mathrm{N/m^2}$ Comparing Fig. 9a and Fig. 9b, one can see that the deflection variations for isotropic and orthotropic non-homogeneous shells are similar. A similar phenomenon has been observed in Fig. 7 for isotropic and orthotropic homogeneous shells.

The variations of the bending moment M_{11} are presented in Fig. 10a and Fig. 10b for isotropic and orthotropic shells, respectively. Here, the bending moments are normalized by the central bending moment value corresponding to a homogeneous isotropic plate $M_{11}^{plate}(a/2) = 0.4634Nm$. The bending moments in homogeneous and FGM shells are almost the same for both isotropic and orthotropic cases. Minimal differences between them are caused by numerical inaccuracies. How-

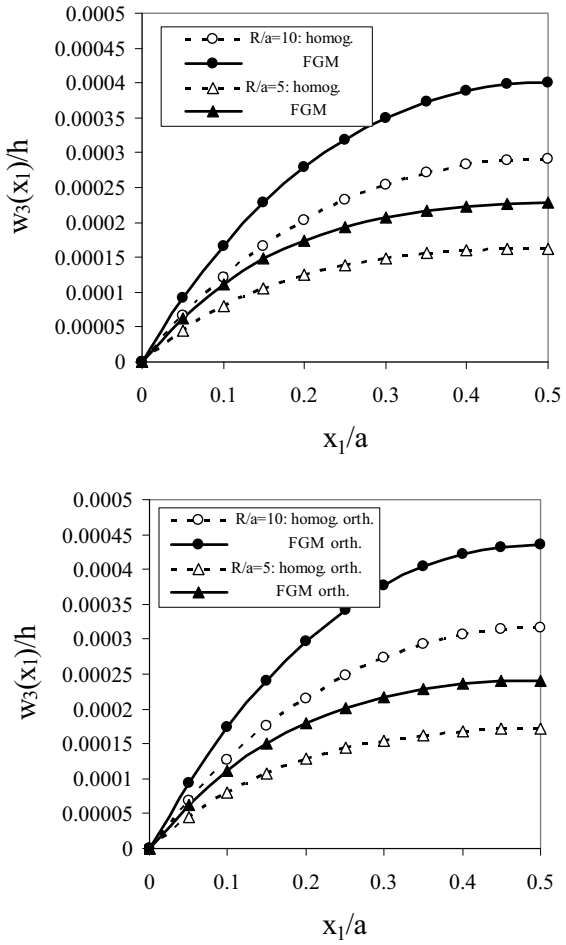

Figure 9: Variation of the deflections with thex_1-coordinate for a simply supported square shallow shell with FGM properties a) isotropic b) orthotropic

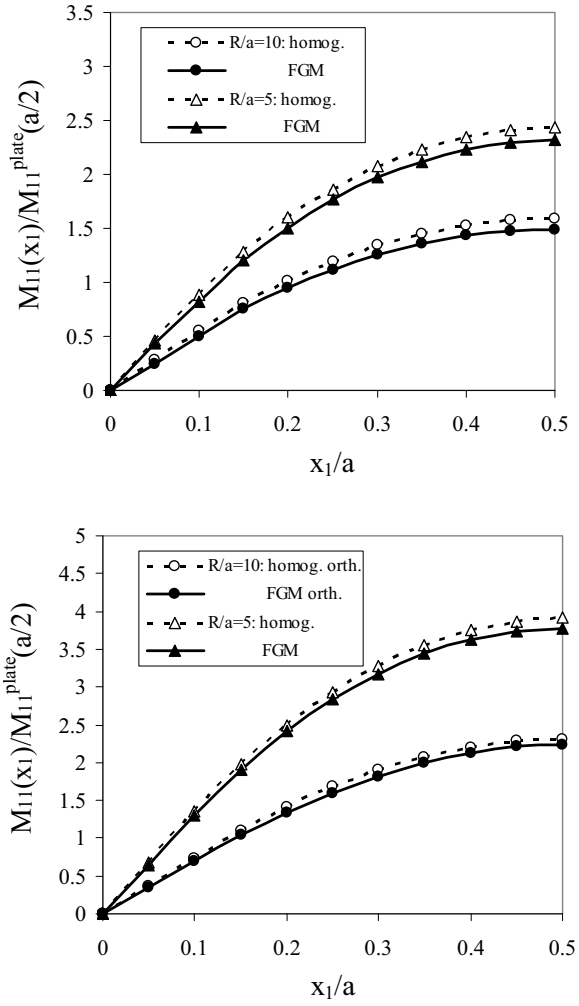

Figure 10: Variation of the bending moments with the x_1-coordinate for a simply supported square shallow shell with FGM properties a) isotropic b) orthotropic

ever, the bending moments are larger for an orthotropic shell than for isotropic one.

In the next example a thermal shock $\theta = H(t-0)$ with Heaviside time variation is applied on the top surface of the shallow shell. If the lateral ends of the shell are thermally insulated, a uniform temperature distribution on shell surfaces is given. The bottom surface is thermally insulated too. The problem can be considered as 1-D in the direction perpendicular to the basic plane of the shell. In such a case the temperature distribution is given by [Carslaw and Jaeger, 1959]

$$\theta(x_3,t) = 1 - \frac{4}{\pi}\sum_{n=0}^{\infty}\frac{(-1)^n}{2n+1}\exp\left[-\frac{(2n+1)^2\pi^2\kappa t}{4h^2}\right] \cos\frac{(2n+1)\pi x_3}{2h}, \quad (49)$$

where the diffusivity coefficient $\kappa = \lambda/\rho c$, with thermal conductivity $\lambda = 100W/m\deg$, mass density $\rho = 7500kg/m^3$ and specific heat $c = 400Ws/kg\deg$. Isotropic material parameters and the thermal expansion coefficients are considered.

The numerical results for the central shell deflection are presented in Fig. 11. Two different

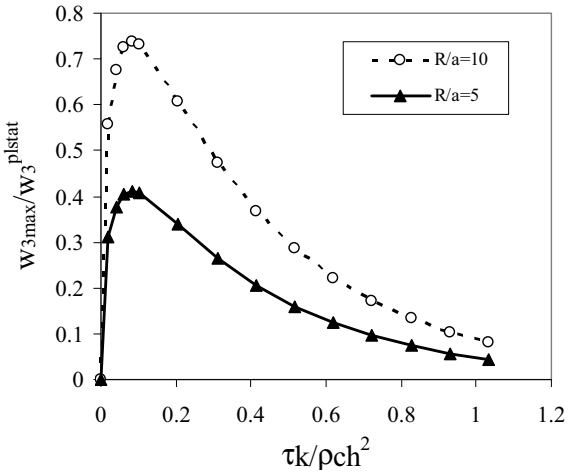

Figure 11: Time variation of the central deflection in the shell

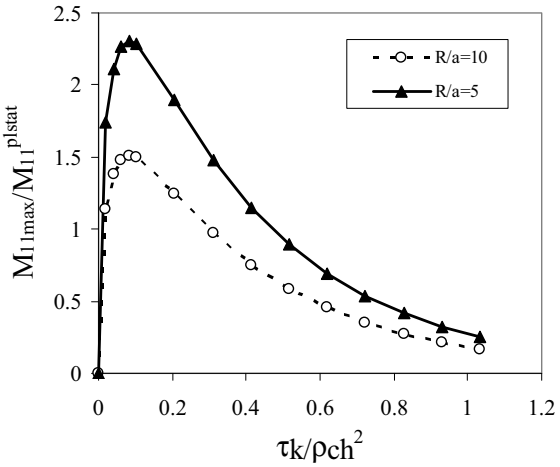

Figure 12: Time variation of the bending moment

shell curvatures are considered here. The deflections are normalized by the central deflection corresponding to the stationary thermal distribution with $\theta = 1\,\mathrm{deg}$ on the top plate surface and vanishing temperature on the bottom surface. For homogeneous material properties the corresponding stationary deflection is $w_3^{plstat} = 0.4829 \cdot 10^{-5} m$. One can observe that in the whole time interval deflections for both shells are lower than in a stationary case. The stiffness of the shell is higher than for a corresponding plate. The deflection is approaching to zero for a large time since thermal forces are vanishing. The temperature distribution is going to be uniform in the whole shell with increasing time.

The bending moment at the center of the plate $M_{11}^{plstat} = 0.4634 Nm$ is used as a normalized parameter in Fig. 12. The time variations of bending moments for the shells of both curvatures are similar. The peak value of the bending moment is larger for larger curvature of the shell. The same phenomenon is observed for a stationary thermal load presented in Fig. 10.

In the last numerical example a clamped square shallow shell is considered. The same geometrical and material parameters as in the above analyzed simply supported shell are considered. Also the same nodal distribution is used in the numerical analysis. We have considered following spatial distribution of temperature on top surface of the shell:

$$\theta(x_1, x_2) = \sin\frac{\pi x_1}{a} \sin\frac{\pi x_2}{a}. \tag{50}$$

The bottom side of the shell is kept at vanishing temperature. A linear variation of temperature through the shell thickness is assumed. Both variants of isotropic and orthotropic material properties are considered here.

The variations of the deflections with the x_1-coordinate are presented in Fig. 13a and Fig. 13b for isotropic and orthotropic shells, respectively. Both figures for isotropic and orthotropic material properties are similar. Counterpart to a mechanical load of an orthotropic shell the deflections are independent on the ratio of Young‘s moduli in orthotropic material. Increasing Young‘s modulus enlarges the thermal forces and flexural rigidity of the shell. Both effects are mutually eliminated in the deformation of shell.

Also functionally graded material properties through the shell thickness are considered. The variation of material properties for the FGM shell is here the same as for a simply supported shell analyzed in the previous example. Since Young's modulus on the bottom side is considered to be smaller than on the top one, the deflection for the FGM shell is larger than for the homogeneous shell with material properties corresponding to the top side.

The variations of the bending moments M_{11} are

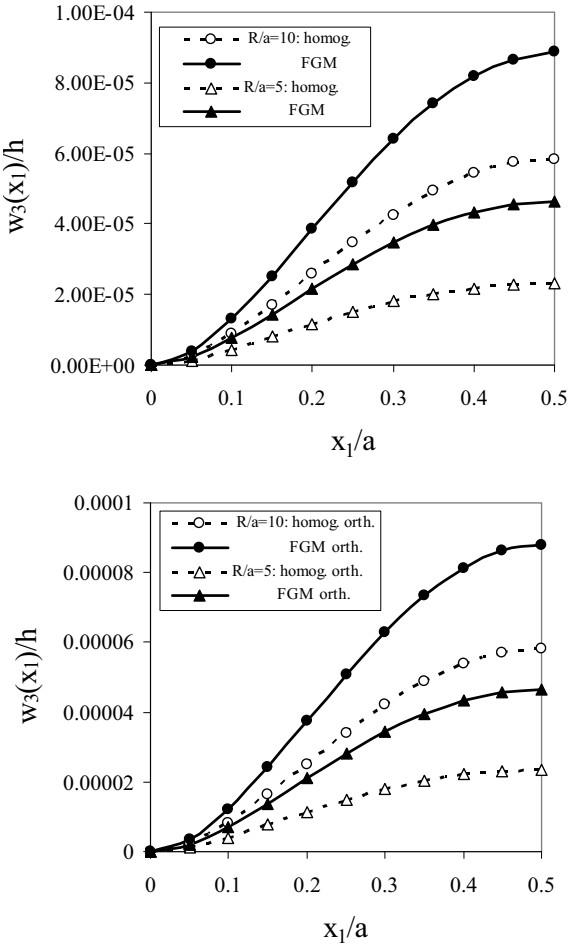

Figure 13: Variation of the deflection with the x_1-coordinate for a clamped square shallow shell a) isotropic b) orthotropic

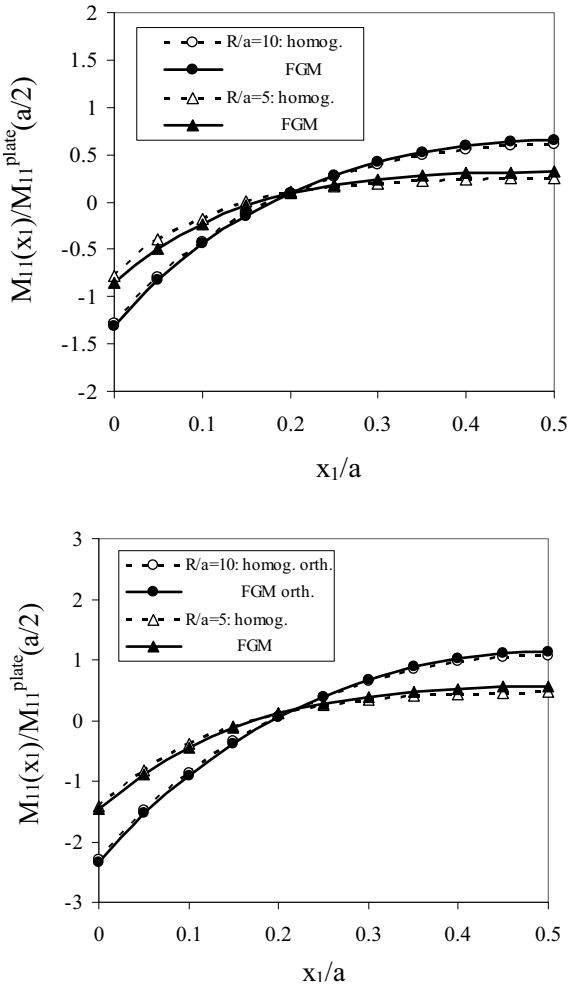

Figure 14: Variation of the bending moment with the x_1-coordinate for a clamped square shallow shell

presented in Fig. 14a and Fig. 14b for isotropic and orthotropic shells, respectively. Here, the bending moments are normalized by the central bending moment value corresponding to a homogeneous isotropic clamped plate $M_{11}^{plate}(a/2) = 0.4769Nm$.

The bending moments in homogeneous and FGM shells are almost the same for both isotropic and orthotropic cases. Minimal differences between them are caused by numerical inaccuracies. Larger bending moments at the fixed part of the orthotropic shell are caused by larger thermal forces. Orthotropic mechanical properties enlarge the bending moments at both places (fixed part and center of shell) for considered shell curvatures. The curvature has an opposite influence on values of the bending moment for a clamped than for a simply supported shell. With increasing shell curvature the value of the bending moment decreases for a clamped shell.

6 Conclusions

The following conclusions can be drawn from the present study:

A meshless local Petrov-Galerkin method is applied to orthotropic shallow shells under a thermal load. Material properties are continuously varying along the shell thickness. The behaviour of the shell is described by the Reissner-Mindlin theory,

which takes the shear deformation into account.

The temperature distribution in shells is determined by the heat conduction equation. The Laplace-transform technique is applied to eliminate the time variable in the considered diffusion equation. The MLPG method for 3-D problem is used to solve the governing equation in the Laplace transform space.

Thermal changes in solids are relatively slow with respect to elastic wave velocity. Therefore, mechanical quantities are described by quasi-static governing equation following from Reissner-Mindlin theory with time playing the role of monotonic parameter. The MLPG method is applied to solve this problem. The analyzed domain is divided into small overlapping circular subdomains. A unit step function is used as the test function in the local weak-form. The derived local boundary-domain integral equations are nonsingular. The Moving Least-Squares (MLS) scheme is adopted for approximating the physical quantities.

The main advantage of the present method is its simplicity and generality. The use of constant test function here is simplest choice, which makes the formulation much simpler than the BEM formulation utilizing the fundamental solution for orthotropic shells. Therefore, the method seems to be promising for problems, which cannot be solved by the conventional BEM due to unavailable fundamental solutions.

The proposed method can be further extended to nonlinear problems, where meshless approximations may have certain advantages over the conventional domain-type discretization approaches.

Acknowledgement: The authors acknowledge the support by the Slovak Science and Technology Assistance Agency registered under number APVV-51-021205, the Slovak Grant Agency VEGA-2/6109/27, VEGA-1/4128/07, and the EPSRC research grant (U.K.) EP/E050573/1.

References

Andreaus, U.; Batra, R.C.; Porfiri, M. (2005): Vibrations of cracked Euler-Bernoulli beams using Meshless Local Petrov-Galerkin (MLPG) method. *CMES: Computer Modeling in Engineering & Sciences*, 9 (2): 111-131.

Arciniega, R.A.; Reddy, J.N. (2007): Tensor-based finite element formulation for geometrically nonlinear analysis of shell structures. *Computer Methods in Applied Mechanics and Engineering*, 196: 1048-1073.

Atluri, S.N., and Zhu, T. (1998): A new Meshless Local Petrov-Galerkin (MLPG) approach in computational mechanics, *Computational Mechanics*, 22: 117-127,

Atluri, S.N.; Shen, S. (2002): *The Meshless Local Petrov-Galerkin (MLPG) Method*, Tech Science Press.

Atluri, S.N. (2004): *The Meshless Method , (MLPG) For Domain & BIE Discretizations*, Tech Science Press.

Atluri, S.N.; Han, Z.D.; Shen, S. (2003): Meshless local Petrov-Galerkin (MLPG) approaches for solving the weakly-singular traction & displacement boundary integral equations. *CMES: Computer Modeling in Engineering & Sciences*, 4: 507-516.

Atluri S.N., Han Z.D., Rajendran A.M. (2004): A new implementation of the meshless finite volume method, through the MLPG "Mixed" approach , *CMES: Computer Modeling in Engineering & Sciences*: 6: 491-513.

Atluri, S.N.; Shen, S. (2005): Simulation of a 4^{th} order ODE: Illustartion of various primal & mixed MLPG methods. *CMES: Computer Modeling in Engineering & Sciences*, 7 (3): 241-268.

Atluri, S.N.; Liu, H.T.; Han, Z.D. (2006a): Meshless local Petrov-Galerkin (MLPG) mixed collocation method for elasticity problems. *CMES: Computer Modeling in Engineering & Sciences*, 14 (3): 141-152.

Atluri, S.N.; Liu, H.T.; Han, Z.D. (2006b): Meshless local Petrov-Galerkin (MLPG) mixed finite difference method for solid mechanics. *CMES: Computer Modeling in Engineering & Sciences*, 15 (1): 1-16.

Bapu Rao, M.N. (1979): Thermal bending of thick rectangular plates. *Nuclear Engineering and*

Design, 54: 115-118.

Belytschko, T.; Krogauz, Y.; Organ, D.; Fleming, M.; Krysl, P. (1996): Meshless methods; an overview and recent developments. *Comp. Meth. Appl. Mech. Engn.*, 139: 3-47.

Beskos D.E. (1991): Static and dynamic analysis of shells. In *Boundary Element Analysis of Plates and Shells* (Beskos D.E. ed.). Springer-Verlag: Berlin, 93-140.

Newton, D.A.; Tottenham, H. (1968): Boundary value problems in thin shallow shells of arbitrary plan form. *Journal of Engineering Mathematics*, 2: 211-223.

Boley, B.A.; Weiner J.H. (1960): *Theory of Thermal Stresses*, John Wiley and Sons, New York.

Carslaw, H.S.; Jaeger, J.C. (1959): *Conduction of Heat in Solids*, Clarendon, Oxford.

Chen, J.S.; Wang, H.P. (2000): New boundary condition treatments for meshless computation of contact problems. *Comp. Meth. Appl. Mech. Engn.*, 187: 441-468.

Ching, H.K.; Chen, J.K. (2006): Thermomechanical analysis of functionally graded composites under laser heating by the MLPG method. *CMES: Computer Modeling in Engineering & Sciences*, 13 (3): 199-217.

Das, M.C.; Rath, B.K. (1972): Thermal bending of moderately thick rectangular plates. *AIAA Journal*, 10: 1349-1351.

Dirgantara, T.; Aliabadi, M.H. (1999): A new boundary element formulation for shear deformable shells analysis. *International Journal for Numerical Methods in Engineering*, 45: 1257-1275.

Donning, B.M.; Liu, K.M. (1998): Meshless methods for shear-deformable beams and plates. *Comp. Meth. Appl. Mech. Engn.*, 152: 47-71.

Dvorkin, E.; Bathe, K.J. (1984): A continuum mechanics based four-node shell element for general nonlinear analysis. *Engineering Comput.*, 1: 77-88.

Han, Z.D.; Rajendran, A.N.; Atluri, S.N. (2005): Meshless Local Petrov-Galerkin (MLPG) approaches for solving nonlinear problems with large deformations and rotations. *CMES: Computer Modeling in Engineering & Sciences*, 10 (1): 1-12.

Han, Z.D.; Liu, H.T.; Rajendran, A.N.; Atluri, S.N. (2006): The applications of Meshless Local Petrov-Galerkin (MLPG) approaches in high-speed impact, penetration and perforation problems. *CMES: Computer Modeling in Engineering & Sciences*, 14 (2): 119-128.

Han, Z.D.; Atluri, S.N. (2008a): An MLPG mixed finite volume method, based on independent interpolations of pressure, volumetric and deviatoric velocity - strains, for analyzing Stokes' flow, *CMES: Computer Modeling in Engineering & Sciences*, In Press

Han, Z.D.; Atluri S.N. (2008b): An MLPG mixed finite volume method, based on independent interpolations of pressure, volumetric velocity-strain, deviatoric velocity-strains, and convection terms, for convection-dominated incompressible flows, *CMES: Computer Modeling in Engineering & Sciences*, In Press.

Gao, L.; Liu, K.; Liu, Y. (2006): applications of MLPG method in dynamic fracture problems. *CMES: Computer Modeling in Engineering & Sciences*, 12 (3): 181-195.

Jarak, T.; Soric, J.; Hoster, J. (2007): Analysis of shell deformation responses by the Meshless Local Petrov-Galerkin (MLPG) approach. *CMES: Computer Modeling in Engineering & Sciences*, 18 (3): 235-246.

Johnson, J.N.; Owen, J.M. (2007): A meshless Local Petrov-Galerkin method for magnetic diffusion in non-magnetic conductors. *CMES: Computer Modeling in Engineering & Sciences*, 22 (3): 165-188.

Krysl, P.; Belytschko, T. (1996a): Analysis of thin plates by the element-free Galerkin method, *Computational Mechanics*, 17: 26-35.

Krysl, P.; Belytschko, T. (1996b): Analysis of thin shells by the element-free Galerkin method, *Int. J. Solids and Structures*, 33: 3057-3080.

Li, S.; Hao, W.; Liu, W.K. (2000): Numerical simulations of large deformation of thin shell structures using meshfree methods. *Computational Mechanics*, 25: 102-116.

Lin, J.; Long, S. (1996): Geometrically nonlinear analysis of the shallow shell by the displacement-based boundary element formulation. *Engn. Analysis with Boundary Elements*, 18: 63-70.

Liu, W.K.; Jun, S.; Zhang, S. (1995): Reproducing kernel particle methods. *International Journal for Numerical Methods in Fluids*, 20: 1081-1106.

Long, S.Y.; Atluri, S.N. (2002): A meshless local Petrov Galerkin method for solving the bending problem of a thin plate. *CMES: Computer Modeling in Engineering & Sciences*, 3: 11-51.

Lu, P.; Huang, M. (1992): Boundary element analysis of shallow shells involving shear deformation. *Int. J. Solids and Structures*, 29: 1273-1282.

Lukasiewicz, S. (1979): *Local Loads in Plates and Shells*, Noordhoff, London.

Ma, Q.W. (2007): Numerical generation of freak waves using MLPG-R and QALE-FEM methods. *CMES: Computer Modeling in Engineering & Sciences*, 18 (3): 223-234.

Ma, Q.W. (2008): A new meshless interpolation scheme for MLPG-R method. *CMES: Computer Modeling in Engineering & Sciences*, 23 (2): 75-89.

Miyamoto, Y.; Kaysser, W.A.; Rabin, B.H.; Kawasaki, A.; Ford, R.G. (1999): *Functionally Graded Materials; Design, Processing and Applications*, Kluwer Academic Publishers, Dordrecht.

Mindlin, R.D. (1951): Influence of rotary inertia and shear on flexural motions of isotropic, elastic plates. *Journal of Applied Mechanics ASME*, 18: 31-38.

Nie, Y.F.; Atluri, S.N.; You, C.W. (2006): The optimal radius of the support of radial weights used in Moving Least Squares approximation. *CMES: Computer Modeling in Engineering & Sciences*, 12 (2): 137-147.

Noguchi, H.; Kawashima, T.; Miyamura, T. (2000): Element free analyses of shell and spatial structures, *International Journal for Numerical Methods in Engineering*, 47: 1215-1240.

Pecher, R.; Elston, S.; Raynes, P. (2006): Mesh-free solution of Q-tensor equations of nematostatics using the MLPG method. *CMES: Computer Modeling in Engineering & Sciences*, 13 (2): 91-101.

Praveen, G.N.; Reddy, J.N. (1998): Nonlinear transient thermoelastic analysis of functionally graded ceramic-metal plates, *Int. J. Solids and Structures*, 35: 4457-4476.

Providakis, C.P.; Beskos, D. (1991): Free and forced vibration of shallow shells by boundary and interior elements. *Computational Methods in Applied Mechanical Engineering*, 92: 55-74.

Qian, L.F.; Batra, R.C.; Chen, L.M. (2004): Analysis of cylindrical bending thermoelastic deformations of fuctionally graded plates by a meshless local Petrov-Galerkin method. *Computational Mechanics*, 33: 263-273.

Qian, L.F.; Batra R.C. (2005): Three-dimensional transient heat conduction in a functionally graded thick plate with a higher-order plate theory and a meshless local Petrov-Galerkin method. *Computational Mechanics*, 35: 214-226.

Reddy J.N. (1997): *Mechanics of Laminated Composite Plates: Theory and Analysis*. CRC Press, Boca Raton.

Reissner, E. (1946): Stresses and small displacements analysis of shallow shells-II, *Journal Math. Physics*, 25: 279-300.

Sellountos, E.J.; Vavourakis, V.; Polyzos, D. (2005): A new singular/hypersingular MLPG (LBIE) method for 2D elastostatics, *CMES: Computer Modeling in Engineering & Sciences*, 7: 35-48.

Shen, H.S. (2000): Nonlinear analysis of simply supported Reissner-Mindlin plates subjected to lateral pressure and thermal loading and resting on two-parameter elastic foundations. *Engineering Structures*, 23: 1481-1493.

Sladek, J.; Sladek, V.; Mang, H.A. (2002): Meshless formulations for simply supported and clamped plate problems. *Int. J. Num. Meth. Engn*., 55: 359-375.

Sladek, J.; Sladek, V.; Mang, H.A. (2003): Meshless LBIE formulations for simply supported and clamped plates under dynamic load.

Computers and Structures, 81: 1643-1651.

Sladek, J.; Sladek, V.; Krivacek, J.; Wen, P.; Zhang, Ch. (2007a): Meshless Local Petrov-Galerkin (MLPG) method for Reissner-Mindlin plates under dynamic load. *Computer Meth. Appl. Mech. Engn.*, 196: 2681-2691.

Sladek, J.; Sladek, V.; Krivacek, J.; Aliabadi, M.H. (2007b): Local boundary integral equations for orthotropic shallow shells, *Int. J. Solids and Structures*, 44: 2285-2303.

Sladek, J.; Sladek, V.; Zhang, Ch.; Solek, P. (2008a): Static and dynamic analysis of shallow shells with functionally graded and orthotropic material properties. *Mechanics of Advanced Materials and Structures*,15: 142–156.

Sladek, J.; Sladek, V.; Solek, P.; Wen, P.H. (2008b): Thermal bending of Reissner-Mindlin plates by the MLPG. *CMES: Computer Modeling in Engineering & Sciences,* 28: 57-76

Soric, J.; Li, Q.; Atluri, S.N. (2004): Meshless local Petrov-Galerkin (MLPG) formulation for analysis of thick plates. *CMES: Computer Modeling in Engineering & Sciences*, 6: 349-357.

Stehfest, H. (1970): Algorithm 368: numerical inversion of Laplace transform. *Comm. Assoc. Comput. Mach*., 13: 47-49.

Suresh, S.; Mortensen A. (1998): *Fundamentals of Functionally Graded Materials.* Institute of Materials, London.

Tauchert T.R. (1991): Thermally induced flexure, buckling and vibration of plates. *Applied Mechanics Reviews,* 44: 347-360.

Vel, S.S.; Batra, R.C. (2002): Exact solution for thermoelastic deformations of functionally graded thick rectangular plates. *AIAA Journal*, 40: 1421-1433.

Wang, J.; Schweizerhof, K. (1996a): Boundary integral equation formulation for moderately thick laminated orthotropic shallow shells. *Computers and Structures*, 58: 277-287.

Wang, J.; Schweizerhof, K. (1996b): Boundary-domain element method for free vibration of moderately thick laminated orthotropic shallow shells. *Int. J. Solids and Structures*, 33: 11-18.

Wu, X.H.; Shen, S.P.; Tao, W.Q. (2007): Meshless Local Petrov-Galerkin collocation method for two-dimensional heat conduction problems. *CMES: Computer Modeling in Engineering & Sciences*, 22 (1): 65-76.

Yuan, W.; Chen, P.; Liu, K. (2007): A new quasi-unsymmetric sparse linear systems solver for Meshless Local Petrov-Galerkin method (MLPG). *CMES: Computer Modeling in Engineering & Sciences*, 17 (2): 115-134.

Zhang, J.D.; Atluri, S.N. (1986): A boundary/interior element method for quasi static and transient response analysis of shallow shells. *Computers and Structures*, 24: 213-223.